The 2012 World Congress on
Advances in Civil, Environmental, and Materials Research (ACEM' 12)
Seoul, Korea, August 26-30, 2012

Nonlinearly Coupled Thermo-Electro-Mechanics and Multi-Field FE Analysis of Thin-walled Structures

R. Schmidt[1)], M. N. Rao[2)] and T.D. Vu[3)]

Institute of General Mechanics, RWTH Aachen University, 52056 Aachen, Germany
[1)] schmidt@iam.rwth-aachen.de,
[2)] rao@iam.rwth-aachen.de, [3)] vu@iam.rwth-aachen.de

ABSTRACT

This paper deals with the continuum mechanics of nonlinear thermo-piezo-elasticity, the transition to a 2-D formulation based on the First-Order Transverse Shear Deformation hypothesis, and its application to coupled nonlinear FE analysis of thin-walled structures. A thermodynamically consistent continuum mechanics based framework that includes the fully nonlinear thermo-piezo-mechanical coupling effects is used. A finite element concept based on weak formulations of the conditions of equilibrium, conservation of electric charge and mechanical energy is applied. The fully geometrically nonlinear shell theory accounts for small strains and finite rotations, as well as for the nonlinear coupling effects between the mechanical, electrical and thermal variables. Numerical examples are shown for a composite plate with piezoelectric layers subjected to a thermal shock.

1. INTRODUCTION

Due to the increasing interest in integrating smart materials into structures for shape and vibration control, many models describing their behaviour have been developed with varying levels of simplification. In the vast majority of papers available in literature coupling of the mechanical, electrical, and eventually thermal field quantities is taken into account in the constitutive equations only. The truly coupled thermo-piezo-elastic analysis, however, does not only consider the temperature and piezoelectric effect on the strains, but accounts for the coupling effects of the mechanical, electrical and thermal quantities in the field equations.

[1)] Professor Dr.-Ing.
[2)] M.Sc.
[3)] Dr.-Ing.

It is well known that due to thermo-elastic coupling structures exhibit several nonclassical physical effects, like e.g. strain rate dependent change of temperature due to tension and compression or damping of vibrations due to heat loss. Nonlinear first-order transverse shear deformation (FOSD) theories of plates and shells, which account for these thermo-elastic coupling effects, and coupled FE simulations have been presented in our earlier works [1, 2, 3]. If additionally piezoelectricity is considered, electro-elastic and thermo-electric coupling effects occur, e.g. the heat conduction equation will depend on the mechanical as well as on the electrical field variables. Thermoelectroelasticity theory has been treated e.g. by Tiersten [4] and Nowacki [5], but only in a few papers on smart structures the attempt is made to take the thermo-piezo-elastic coupling into account, like in Görnandt and Gabbert [6], Ahmad, Upadhyay and Venkatesan [7, 8].
In the present paper an extension of our previous works [1, 2, 3] is used for a thermodynamically consistent continuum mechanics based framework including the conservation of mass, linear and angular momentum, electric charge and energy [9-13]. The second principle of thermodynamics is used to derive the restrictions for the constitutive equations using the Coleman-Noll analysis approach. The resulting set of 3-D field equations accounts for the geometrical, electrical and thermal nonlinear effects, the thermo-electro-mechanical coupling effects, as well as the instationary thermal and electric effects. It is more general and valid for a wider class of problems than most models published in literature. A finite element concept based on weak formulations of the conditions of equilibrium, conservation of electric charge and energy is used. Transition from 3-D continuum mechanics to 2-D theories of plates and shells is performed in the framework of the Reissner-Mindlin hypothesis.
A nonlinear FE code for multi-field analysis of coupled thermo-piezo-elastic shell problems has been developed in by Lentzen [13], and will be used throughout this paper. Various nonlinear and coupling effects are demonstrated for a piezolaminated steel plate subjected to thermal shock.

2. CONSERVATION LAWS

In this chapter we summarize the conservation laws of nonlinear themopiezoelasticity as derived in [1] for fully coupled thermoelasticity and extended in [13] by the electric field variables (see also [2-3,9-13b]). In this formulation no linearization, e.g. to small displacements or small temperature differences has been made.

Conservation of mass:

$$d\bar{m} = dm \quad \Rightarrow \quad \bar{\rho}\sqrt{\bar{g}} = \rho\sqrt{g} \tag{1}$$

Conservation of linear momentum:

$$\tau^{im}\|_i + \bar{p}^i \bar{E}^m \|_i + \bar{\rho}\,\bar{B}^m = \bar{\rho}\,\bar{A}^m \tag{2}$$

Conservation of angular momentum:

$$(\tau^{im} + \bar{p}^{i}\bar{E}^{m})\bar{\mathbf{g}}_i \times \bar{\mathbf{g}}_m = 0 \quad \Rightarrow \quad \tau^{[im]} + \bar{p}^{[i}\bar{E}^{m]} = 0 \tag{3}$$

Gauss' law:

$$\bar{D}^{i}\,\|_{i} = 0 \tag{4}$$

Conservation of energy (first principle of thermodynamics):

$$DU = DW + DW_e + DQ \quad \Rightarrow \quad \bar{\rho}\dot{\bar{u}} = (\tau^{(im)} + \bar{p}^{(i}\bar{E}^{m)})\dot{E}_{im} + \bar{\rho}\dot{E}_i\dot{\bar{\pi}}^{i} + \bar{\rho}\bar{h} - \bar{h}^{k}\,\|_{k} \tag{5}$$

Here, an overbar indicates the deformed configuration, $\boldsymbol{g}_i$ (i = 1, 2, 3), g, ρ, m denote the covariant base vectors, the metric tensor determinant, density and mass, respectively, B^m and A^m are the body force and acceleration vector components, U, W, W_e and Q stand for the internal energy, the mechanical work, the electrical work and the thermal energy, τ^{im}, E_{im} and E^m are the components of the Cauchy stress, the fully nonlinear Green-Lagrange strain tensor and the spatial electric field, h^k and h denote the heat flux and the internal heat source, while $(..)\|_i$ is the covariant derivative with respect to the deformed curvilinear coordinates θ^{ji}, and a dot denotes the time derivative.

3. SECOND LAW OF THERMODYNAMICS

The first and the second Clausius-Duhem inequality can be summarized as Meixner inequality

$$-\left(\frac{\bar{h}^{k}}{T}\right)\Big\|_{k} + \bar{\rho}\frac{\bar{h}}{T} \le \bar{\rho}\dot{\bar{s}} \tag{6}$$

where T denotes the temperature and s is the entropy density. After employing the first principle of thermodynamics Eq. (5), it can be written as

$$\bar{\rho}\dot{\bar{u}} - (\tau^{(im)} + \bar{p}^{(i}\bar{E}^{m)})\dot{E}_{im} - \bar{\rho}\dot{E}_i\dot{\bar{\pi}}^{i} + \frac{\bar{h}^{k}}{T}T_{,k} \le \bar{\rho}\dot{\bar{s}}T \tag{7}$$

or using the Gibbs free energy

$$\bar{G} = \bar{u} - \bar{\pi}^i \bar{E}_i - T\bar{s} \tag{8}$$

in the form

$$\bar{\rho}\dot{\bar{G}} - (\tau^{(im)} + \bar{p}^{(i}\bar{E}^{m)})\dot{E}_{im} - \bar{\rho}\bar{\pi}^i \dot{\bar{E}}_i + \frac{\bar{h}^k}{T} T_{,k} \le -\bar{\rho}\bar{s}\dot{T} \tag{9}$$

where $(..)_{,k}$ denotes the partial derivative along θ^k. In what follows we assume that all derived variables (τ^{ik} , $\bar{h}^k$, $\bar{s}$, $\bar{p}^k$) depend on $\bar{\rho}$, $E_{ik}, \bar{E}_i$, $\bar{E}_{i,k}$, T and $T_{,k}$. This is sufficient to account for the effects of thermoelastic coupling, thermoelectric coupling and instationary heat flux. With this assumption Eq. (9) yields the following restrictions for the constitutive equations:

$$\dot{\bar{\rho}} : \frac{\partial \bar{G}}{\partial \bar{\rho}} = 0, \quad \dot{\bar{E}}_{i,k} : \frac{\partial \bar{G}}{\partial \bar{E}_{i,k}} = 0, \quad \dot{T}_k : \frac{\partial \bar{G}}{\partial T_{,k}} = 0 \Rightarrow \quad \bar{G} = \bar{G}\left(\bar{E}_{ik}, \bar{E}_i, T\right)$$

$$\dot{E}_{ik} : \tau^{(ik)} = \bar{\rho}\frac{\partial \bar{G}}{\partial E_{ik}} - p^{(i}E^{k)}, \quad \dot{\bar{E}}_i : \bar{p}^i = -\bar{\rho}\frac{\partial \bar{G}}{\partial \bar{E}_i}, \quad \dot{T} : \bar{s} = -\frac{\partial \bar{G}}{\partial T} \quad \text{and:} \quad \frac{\bar{h}^k}{T} T_{,k} \le 0 \tag{10}$$

If these restrictions are taken into account in Eq.(5), the first principle of thermodynamics assumes the form

$$-\bar{h}^k \|_k + \bar{\rho}\bar{h} = \bar{\rho}T\dot{\bar{s}} \tag{11}$$

4. CONSTITUTIVE EQUATIONS

For the Gibbs free energy we assume the form

$$\rho\bar{G} = \frac{1}{2}c^{ijkl}E_{ij}E_{kl} + \frac{1}{2}d^{ik}E_iE_k - e^{jik}E_jE_{ik} + f^j\Delta TE_j - a^{ik}\Delta TE_{ik} - \beta g\left(T\right) \tag{12}$$

where $\Delta T = T - T_0$, T_0 is the initial temperature, e^{jik} are the piezoelectric coupling coefficients, d^{ik} are the electric permittivity coefficients and f^j are the pyroelectric coefficients. It can be shown that β becomes identical with the heat capacity at constant strain ($\beta = c_E$) if we choose $g\left(T\right) = \rho\left[T\left(\ln\frac{T}{T_0} - 1\right) + T_0\right]$. Applying the restrictions imposed by the second law of thermodynamics we get now the following constitutive equations for isotropic materials:

$$\sqrt{\frac{\bar{g}}{g}}\tau^{ij} = \frac{1}{2}c^{ijkl}E_{kl} - \alpha^{ij}\Delta T - e^{kij}E_k - \rho E^{(i}\pi^{j)} \tag{13}$$

with

$$c^{ijkl} = \lambda g^{ij}g^{kl} + 2Gg^{ik}g^{jl}, \quad \alpha^{ij} = \alpha_T c^{ijkl}g_{kl} \tag{14}$$

and

$$\bar{s} = \frac{1}{\rho}\alpha_T E_s^s + c_E \ln\frac{T}{T_0} - \frac{1}{\rho}f^i E_i \tag{15}$$

$$\bar{p}^k = d^{ki}E_i - e^{kij}E_{ij} - f^k\Delta T \tag{16}$$

$$\sqrt{\frac{\bar{g}}{g}}\bar{h}^k = -\lambda_T g^{ks}T_{,s} \tag{17}$$

Here λ and G are Lamé's constants, α_T is the thermal expansion coefficient, and λ_T is the heat conductivity coefficient. With Eqs.(15,17) the first principle of thermodynamics (Eq.(5)) yields

$$\lambda_T G^k\big|_k = \alpha_T T\dot{E}_s^s + \rho f^i T\dot{E}_i + \rho c_E\dot{T} - \rho h \tag{18}$$

where $G^k = g^{ks}T_{,s}$ is the temperature gradient and $(..)|_k$ stands for the covariant derivative with respect to the undeformed configuration. Eq.(18) is the instationary heat conduction equation. It can be seen that the right-hand side depends not only on the temperature but also on the mechanical and electrical field variables, more precisely on the strain rates and the electric field rates. The first term is the thermoelastic coupling term, the second one is the thermoelectric coupling term. It should be mentioned that in both terms the actual temperature T appears. Thus, coupling is taken into account in a fully nonlinear way, in contrast to many other papers where due to earlier simplifications only the initial temperature appears instead of the actual one.

5. VARIATIONAL FORMULATION

Starting from Eq.(2), the virtual work generated by a virtual displacement δv_m is

$$\delta W = \int_{\bar{v}}\left(\tau^{im}\big\|_i + \bar{\rho}\left(\bar{B}^m - \bar{A}^m\right)\right)\delta v_m \, d\bar{V} \tag{19}$$

Applying Gauss' divergence theorem and relating all quantities to the undeformed configuration leads to

$$\int_V s^{im}\delta E_{im}\, dV - \int_V \rho\left(B^m - A^m\right)\delta v_m\, dV - \int_B s^m \delta v_m\, dB = 0 \qquad (20)$$

where s^{im} denotes the 2nd Piola-Kirchhoff stress tensor components and s^m the traction vector components on the boundary. Similarly, with the assumption of no entropy production and no internal heat source Eq.(11) multiplied by δT and integrated over the deformed body leads to the second weak formulation

$$\int_{\bar{V}}\left(\bar{\rho}\bar{h} - \bar{h}^k\,\|_k - \bar{\rho}T\dot{\bar{s}}\right)\delta T\, d\bar{V} = \int_V h^k \delta T_{,k}\, dV + \int_V\left(\rho h - \rho T\dot{s}\right)\delta T\, dV - \int_B h^k n_k \delta T\, dB = 0 \qquad (21)$$

where n_k are the components of the normal vector of the undeformed boundary surface.

The weak form of Gauss' law is

$$\int_{\bar{V}} \bar{D}^i\,\|_i\, \delta\bar{\varphi}\, d\bar{V} = -\int_V D^i \delta E_i\, dV + \int_B D^i n_i\, \delta\varphi\, dB = 0 \qquad (21)$$

where φ denotes the electric potential.

6. FINITE ROTATION SHELL THEORY AND FINITE ELEMENT METHOD

Based on the weak formulations Eqs. (9) - (11), the transition from 3-D continuum mechanics to fully geometrically nonlinear 2-D theories of plates and shells is performed by using the First-order Transverse Shear Deformation (FOSD) hypothesis, while the transverse electric potential and temperature distribution are assumed to be quadratic and cubic, respectively. The latter is chosen such that various boundary conditions can be accurately imposed, including adiabatic surfaces.

The finite element developed by Lentzen in [13] is based on the Hu-Washizu shell element of Gruttmann and Wagner [14] and extended with the thermoelectrical coupling. In the present element a displacement based variational principle is chosen in order to reduce the number of internal variables. In order to overcome various types of locking, ANS combined with an EAS procedure has been used.

There are no kinematical restrictions with respect to the range of strains and rotations. The director is assumed to be inextensible, the rotations are parametrised with the Rodriguez formulation. In order to overcome various types of locking, ANS combined with an EAS procedure has been used.

6.*1. Kinematical relations*

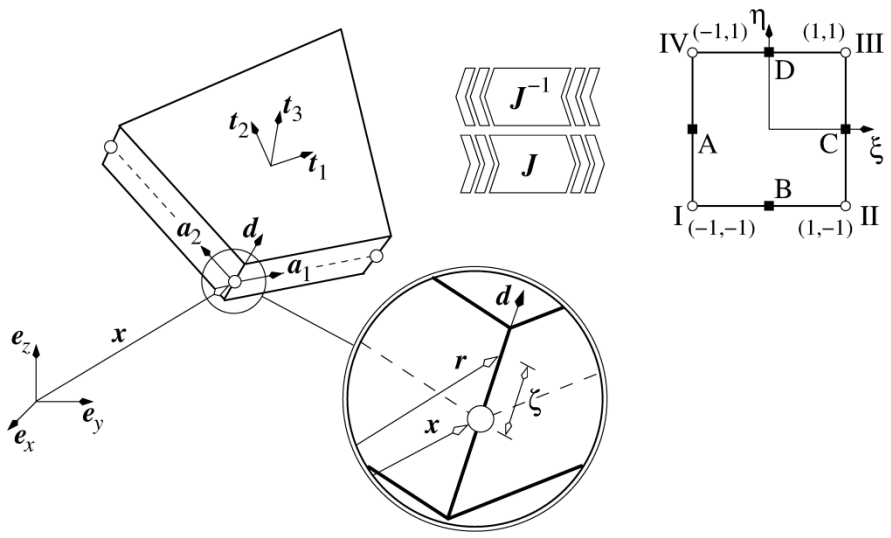

Fig. 1 Definition of the coordinate systems in the FRT-element.

Fig. 1 shows the four-node element with the global e_i, the local a_α, the natural $\xi-\eta$ and the orthonormal material t_i coordinate system. The local coordinate system is used optionally in case the drilling rotation is enforced to vanish, or when specific rotation boundary conditions are required. Both the local as well as the material coordinate system can be prescribed by the input given that t_3 is perpendicular to the reference surface at the centre of the element. The material coordinate system can additionally be automatically generated as

$$\hat{t}_1 = \frac{x_3 - x_1}{|x_3 - x_1|} + \frac{x_2 - x_4}{|x_2 - x_4|} \tag{22}$$

$$\hat{t}_2 = \frac{x_3 - x_1}{|x_3 - x_1|} - \frac{x_2 - x_4}{|x_2 - x_4|} \tag{23}$$

$$t_3 = t_1 \times t_2 \text{ with } t_1 = \frac{\hat{t}_1}{|\hat{t}_1|} \text{ and } t_2 = \frac{\hat{t}_2}{|\hat{t}_2|} \tag{24}$$

The position vector to the reference surface in the initial configuration at node *I* is denoted as x_I.

Fig. 1 also shows that a linear displacement field is assumed by introducing the inextensible director *d* which is a unit vector perpendicular to the reference surface in the un-deformed configuration.

The FOSD hypothesis reads for the covariant components of the displacements vector reads

$$v_\alpha = \overset{0}{v}_\alpha + \zeta \overset{1}{v}_\alpha, \quad v_3 = \overset{0}{v}_3 + \zeta \overset{1}{v}_3 \tag{25}$$

In the framework of this hypothesis the Green strain-tensor components and fully nonlinear finite rotation strain-displacement relations are obtained as (see [15], [16])

$$E_{\alpha\beta} = \overset{0}{E}_{\alpha\beta} + \zeta \overset{1}{E}_{\alpha\beta} + \zeta^2 \overset{2}{E}_{\alpha\beta} \tag{26}$$

$$E_{\alpha 3} = \overset{0}{E}_{\alpha 3} + \zeta \overset{1}{E}_{\alpha 3} \tag{27}$$

$$E_{33} = 0 \tag{28}$$

with

$$\overset{0}{E}_{\alpha\beta} = \frac{1}{2}\left(\overset{0}{\varphi}_{\alpha\beta} + \overset{0}{\varphi}_{\beta\alpha} \right) + \underline{\frac{1}{2} \overset{0}{\varphi}_{\alpha 3} \overset{0}{\varphi}_{\beta 3}} + \underline{\underline{\frac{1}{2} \overset{0}{\varphi}_{\lambda\alpha} \overset{0}{\varphi}^{\lambda}_{\bullet\beta}}} \tag{29}$$

$$\begin{aligned} \overset{1}{E}_{\alpha\beta} = {} & \frac{1}{2}\left(\overset{1}{\varphi}_{\alpha\beta} + \overset{1}{\varphi}_{\beta\alpha} \right) - \frac{1}{2}\left(b^{\lambda}_{\alpha} \overset{0}{\varphi}_{\lambda\beta} + b^{\lambda}_{\beta} \overset{0}{\varphi}_{\lambda\alpha} \right) + \underline{\frac{1}{2}\left(\overset{0}{\varphi}_{\alpha 3} \overset{1}{\varphi}_{\beta 3} + \overset{0}{\varphi}_{\beta 3} \overset{1}{\varphi}_{\alpha 3} \right)} \\ & + \underline{\underline{\frac{1}{2}\left(\overset{0}{\varphi}_{\lambda\alpha} \overset{1}{\varphi}^{\lambda}_{\bullet\beta} + \overset{1}{\varphi}_{\lambda\alpha} \overset{0}{\varphi}^{\lambda}_{\bullet\beta} \right)}} \end{aligned} \tag{30}$$

$$\overset{2}{E}_{\alpha\beta} = -\frac{1}{2}\left(b^{\lambda}_{\alpha} \overset{1}{\varphi}_{\lambda\beta} + b^{\lambda}_{\beta} \overset{1}{\varphi}_{\lambda\alpha} \right) + \underline{\frac{1}{2} \overset{1}{\varphi}_{\alpha 3} \overset{1}{\varphi}_{\beta 3}} + \underline{\underline{\frac{1}{2} \overset{1}{\varphi}_{\lambda\alpha} \overset{1}{\varphi}^{\lambda}_{\bullet\beta}}} \tag{31}$$

$$2\overset{0}{E}_{\alpha 3} = \overset{0}{\varphi}_{\alpha 3} + \overset{1}{\upsilon}_{\alpha} + \underline{\overset{1}{\upsilon}^{\lambda} \overset{0}{\varphi}_{\lambda\alpha} + \frac{1}{2} \overset{1}{\upsilon}_3 \left(\overset{0}{\varphi}_{\lambda 3} - \overset{1}{\upsilon}_{\alpha} \right)} + \underline{\underline{\frac{1}{2} \overset{1}{\upsilon}_3 \left(\overset{0}{\varphi}_{\lambda 3} + \overset{1}{\upsilon}_{\alpha} \right)}} \tag{32}$$

$$2\overset{1}{E}_{\alpha 3} = \overset{1}{\upsilon}_{3,\alpha} + \underline{\overset{1}{\upsilon}^{\lambda} \overset{1}{\upsilon}_{\lambda|\alpha} - \frac{1}{2} \overset{1}{\upsilon}_{3,\lambda} \overset{0}{\varphi}^{\lambda}_{\bullet\alpha}} + \underline{\underline{\overset{1}{\upsilon}_3 \overset{1}{\upsilon}_{3,\alpha} + \frac{1}{2} \overset{1}{\upsilon}_{3,\lambda} \overset{0}{\varphi}^{\lambda}_{\bullet\alpha}}} \tag{33}$$

If all underlined terms are dropped one obtains the geometrically linear theory, if the terms marked by a double line are dropped one obtains the nonlinear moderate rotation theory. We refer to [16] for the abbreviations used in Eqs. (29-33).

In the following, the partial derivatives with respect to the natural coordinate system are denoted by $\square_{,\alpha}$ and those with respect to the material coordinate system by $\square_{,i}$.

Due to the thinness of the regarded shells, the components $\overset{2}{E}_{\alpha\beta}$ and $\overset{1}{E}_{\alpha 3}$ are neglected.

6.*2. Electric potential distribution*

For this finite element, the electric potential is assumed to vary quadratically through the thickness. For each piezoelectric layer a quadratic polynomial is assumed introducing three electrical degrees of freedom per layer

$$\varphi(\zeta) = \overset{0}{\varphi} + \zeta \overset{1}{\varphi} + \zeta^2 \overset{2}{\varphi} \tag{34}$$

The above introduced degrees of freedom are not very well manageable in the finite element application. For instance the boundary conditions on the bottom and the top electrode of the piezoelectric layers cannot be easily defined, and moreover these quantities can generally not be physically interpreted. Therefore the above mentioned electrical degree of freedom are converted into the electric potential on the lower electrode, in the middle of the piezoelectric layer and to the top electrode, respectively denoted by $\overset{-}{\psi}$, $\overset{m}{\psi}$, $\overset{+}{\psi}$. The conversion is performed by inverting the following matrix-vector representation of the boundary conditions

$$\begin{Bmatrix} \overset{-}{\varphi} \\ \overset{m}{\varphi} \\ \overset{+}{\varphi} \end{Bmatrix} = \begin{pmatrix} 1 & \overset{-}{\zeta} & \overset{-}{\zeta}^2 \\ 1 & \overset{m}{\zeta} & \overset{m}{\zeta}^2 \\ 1 & \overset{+}{\zeta} & \overset{+}{\zeta}^2 \end{pmatrix} \begin{Bmatrix} \overset{0}{\varphi} \\ \overset{1}{\varphi} \\ \overset{2}{\varphi} \end{Bmatrix} \tag{35}$$

leading to

$$\begin{Bmatrix} \overset{0}{\varphi} \\ \overset{1}{\varphi} \\ \overset{2}{\varphi} \end{Bmatrix} = \frac{1}{k_1} \begin{pmatrix} \overset{m}{\zeta}\overset{+}{\zeta}(\overset{+}{\zeta}-\overset{m}{\zeta}) & \overset{-}{\zeta}\overset{+}{\zeta}(\overset{-}{\zeta}-\overset{+}{\zeta}) & \overset{m}{\zeta}\overset{-}{\zeta}(\overset{m}{\zeta}-\overset{-}{\zeta}) \\ (\overset{+}{\zeta}+\overset{m}{\zeta})(\overset{m}{\zeta}-\overset{-}{\zeta}) & (\overset{+}{\zeta}+\overset{+}{\zeta})(\overset{+}{\zeta}-\overset{-}{\zeta}) & (\overset{m}{\zeta}+\overset{-}{\zeta})(\overset{-}{\zeta}-\overset{m}{\zeta}) \\ (\overset{+}{\zeta}-\overset{m}{\zeta}) & (\overset{+}{\zeta}-\overset{-}{\zeta}) & (\overset{m}{\zeta}-\overset{-}{\zeta}) \end{pmatrix} \begin{Bmatrix} \overset{-}{\varphi} \\ \overset{m}{\varphi} \\ \overset{+}{\varphi} \end{Bmatrix} \tag{36}$$

with $k_1 = \overset{m}{\zeta}\overset{+}{\zeta}^2 - \overset{+}{\zeta}\overset{m}{\zeta}^2 + \overset{+}{\zeta}\overset{-}{\zeta}^2 - \overset{-}{\zeta}\overset{+}{\zeta}^2 + \overset{-}{\zeta}\overset{m}{\zeta}^2 - \overset{m}{\zeta}\overset{-}{\zeta}^2$

The above relation is abbreviated as

$$\{\tilde{\varphi}\} = \left[A^{\varphi}\right]\{\varphi\} \tag{37}$$

6.*3. Temperature difference distribution*

In the present element it is assumed, that the temperature field in the undeformed configuration is homogenous. Therefore the temperature is expressed in temperature differences $\vartheta = T - T_0$. The transverse temperature distribution is assumed to be described by a cubic polynomial

$$\vartheta(\zeta) = \overset{0}{\vartheta} + \zeta \overset{1}{\vartheta} + \zeta^2 \overset{2}{\vartheta} + \zeta^3 \overset{3}{\vartheta} \tag{38}$$

For this description four thermal degrees of freedom $\overset{0}{\vartheta}$, $\overset{1}{\vartheta}$, $\overset{2}{\vartheta}$, $\overset{3}{\vartheta}$ have to be introduced, which are again not very manageable when applied in a finite element method, and a sound physical interpretation is lacking.

More useful is the introduction of the temperature on the bottom and the top bounding surfaces, and the transverse temperature gradients on the bottom and the top bounding surfaces respectively denoted by $\bar{\vartheta}$, $\overset{+}{\vartheta}$, $\bar{e}_3$, $\overset{+}{e}_3$. With these degrees of freedom boundary conditions for the temperature on both surfaces can be enforced, and additionally the heat flux into and out of the shell can be controlled. If, for instance, adiabatic boundary conditions are required, then $\bar{e}_3$ and $\overset{+}{e}_3$ are set equal zero. The conversion from the original set of degrees of freedom to the present one is performed by inverting the following matrix-vector representation of the boundary conditions.

$$\begin{Bmatrix} \bar{\vartheta} \\ \overset{+}{\vartheta} \\ \bar{e}_3 \\ \overset{+}{e}_3 \end{Bmatrix} = \begin{pmatrix} 1 & \bar{\zeta} & \bar{\zeta}^2 & \bar{\zeta}^3 \\ 1 & \overset{+}{\zeta} & \overset{+}{\zeta}^2 & \overset{+}{\zeta}^3 \\ 0 & 1 & 2\bar{\zeta} & 2\bar{\zeta}^2 \\ 0 & 1 & 2\overset{+}{\zeta} & 3\overset{+}{\zeta}^2 \end{pmatrix} \begin{Bmatrix} \overset{0}{\vartheta} \\ \overset{1}{\vartheta} \\ \overset{2}{\vartheta} \\ \overset{3}{\vartheta} \end{Bmatrix} \tag{39}$$

leading to

$$\begin{Bmatrix} \bar{\vartheta} \\ \overset{+}{\vartheta} \\ \bar{e}_3 \\ \overset{+}{e}_3 \end{Bmatrix} = \begin{pmatrix} \frac{\overset{+}{\zeta}^2(3\bar{\zeta} - \overset{+}{\zeta})}{k_1} & \frac{\bar{\zeta}^2(\bar{\zeta} - 3\overset{+}{\zeta})}{k_1} & -\frac{\bar{\zeta}\overset{+}{\zeta}^2}{k_2} & -\frac{\bar{\zeta}\overset{+}{\zeta}^2}{k_2} \\ -\frac{6\bar{\zeta}\overset{+}{\zeta}}{k_1} & -\frac{6\bar{\zeta}\overset{+}{\zeta}}{k_1} & \frac{\overset{+}{\zeta}(2\bar{\zeta} + \overset{+}{\zeta})}{k_2} & \frac{\bar{\zeta}(2\overset{+}{\zeta} + \bar{\zeta})}{k_2} \\ \frac{3(\bar{\zeta} + \overset{+}{\zeta})}{k_1} & -\frac{3(\bar{\zeta} + \overset{+}{\zeta})}{k_1} & -\frac{3(\bar{\zeta} + \overset{+}{\zeta})}{k_2} & -\frac{(\overset{+}{\zeta} + 2\bar{\zeta})}{k_2} \\ -\frac{2}{k_1} & -\frac{2}{k_1} & \frac{1}{k_2} & \frac{1}{k_2} \end{pmatrix} \begin{Bmatrix} \overset{0}{\vartheta} \\ \overset{1}{\vartheta} \\ \overset{2}{\vartheta} \\ \overset{3}{\vartheta} \end{Bmatrix} \tag{40}$$

with $k_1 = (\bar{\zeta} - \overset{+}{\zeta})^3$ and $k_2 = (\bar{\zeta} - \overset{+}{\zeta})^2$

The above relation is abbreviated as

$$\left\{\tilde{\vartheta}\right\} = \left[A^{\vartheta}\right]\{\vartheta\} \tag{41}$$

6.*4. The system matrices and vectors*

The following set of equations can be formulated on element level from the variational formulations

$$\begin{pmatrix} [M_{qq}] & 0 \\ 0 & 0 \end{pmatrix}^e \begin{Bmatrix} \{\ddot{q}\} \\ \{\ddot{\alpha}\} \end{Bmatrix}^e + \begin{pmatrix} [K_{qq}] & [K_{q\alpha}] \\ [K_{\alpha q}] & [K_{\alpha\alpha}] \end{pmatrix}^e \begin{Bmatrix} \{\Delta q\} \\ \{\Delta\alpha\} \end{Bmatrix}^e = \begin{Bmatrix} \{f_q^q\} - \{f_q^i\} \\ -\{f_\alpha^i\} \end{Bmatrix}^e, \tag{42}$$

and

$$\begin{pmatrix} -[D_{qq}] & 0 \\ 0 & 0 \end{pmatrix}^e \begin{Bmatrix} \{\dot{\vartheta}\} \\ \{\dot{\alpha}_e\} \end{Bmatrix}^e + \begin{pmatrix} [K_{\vartheta\vartheta}] & [K_{\vartheta\alpha}] \\ [K_{\alpha\vartheta}] & [K_{\alpha_e\alpha_e}] \end{pmatrix}^e \begin{Bmatrix} \{\Delta\vartheta\} \\ \{\Delta\alpha_e\} \end{Bmatrix}^e = \begin{Bmatrix} \{f_\vartheta^q\} - \{f_\vartheta^i\} \\ -\{f_{\alpha_e}^i\} \end{Bmatrix}^e, \tag{43}$$

The following abbreviations have been used

$$\begin{aligned} \{q\}^T &= \{\{\mathrm{v}_I\}^T, \{\varphi_1^1\}^T, \{\varphi_1^P\}^T, \cdots, \{\mathrm{v}_I\}^T, \{\varphi_4^1\}^T, \{\varphi_4^P\}^T\} \\ \{\vartheta\}^T &= \{\{\vartheta_1\}^T, \cdots, \{\vartheta_4\}^T\} \\ \{\alpha\}^T &= \{\{\alpha_E\}^T, \{\alpha_\varepsilon^1\}^T, \{\alpha_\varepsilon^P\}^T\} \end{aligned} \tag{44}$$

where

$$[K_{qq}]^e = [K^\sigma]^e + \int_{\Omega^e} [B]^T [\mathrm{H}_1][B] d\Omega,\ [K_{q\alpha}]^e = [K_{\alpha q}]^{eT} = \int_{\Omega^e} [B]^T [\mathrm{H}_1][N_q] d\Omega$$

$$[K_{\alpha\alpha}]^e = \int_{\Omega^e} [N_q]^T [\mathrm{H}_1][N_q] d\Omega,\ [K_{\vartheta\alpha}]^e = [K_{\alpha\vartheta}]^{eT} = \int_{\Omega^e} [B^\vartheta]^T [\mathrm{H}_3][N_e] d\Omega$$

$$[K_{\vartheta\vartheta}]^e = \int_{\Omega^e} [B^\vartheta]^T [\mathrm{H}_3][B^\vartheta] d\Omega - \int_{\Omega^e} [N]^T [\mathrm{H}_6][N] d\Omega,$$

$$[K_{\alpha_e\alpha_e}]^e = \int_{\Omega^e} [N_e]^T [\mathrm{H}_3][N_e] d\Omega,\ [D_{\vartheta\vartheta}]^e = \int_{\Omega^e} [N]^T [\mathrm{H}_4][N] d\Omega,$$

The elemental in-balance force vectors are obtained as

$$
\begin{aligned}
\{f_q^i\}^e &= \int_{\Omega^e} [B]^T (\{\hat{\sigma}\}_q + \{\hat{\sigma}\}_\vartheta) d\Omega \\
\{f_\alpha^i\}^e &= \int_{\Omega^e} [N_q]^T (\{\hat{\sigma}\}_q + \{\hat{\sigma}\}_\vartheta) d\Omega \\
\{f_\vartheta^i\}^e &= \int_{\Omega^e} [B^\vartheta]^T \{\hat{h}\} d\Omega - \int_{\Omega^e} [N]^T [\mathrm{H}_5] \{\dot{\hat{\varepsilon}}\} d\Omega \\
\{f_{\alpha_e}^i\}^e &= \int_{\Omega^e} [N_e]^T \{\hat{h}\} d\Omega
\end{aligned}
$$

and further $\left\{f_q^a\right\}$ denotes the standard vector containing the nodal forces, moment and charges, and $\left\{f_\vartheta^a\right\}$ is the vector containing the amounts of heat entering of leaving the body at each node. The dependent quantities denoted by $\hat{\square}$ are obtained with the enhanced independent quantities inserted into the integrated constitutive relations. The integration over the reference surface is conducted with the four-point Gauss quadrature. Since the interpolation of the enhancing quantities is discontinuously across the element boundaries, the parameters $\left\{\Delta\alpha\right\}$ and $\left\{\Delta\alpha_e\right\}$ can be statically condensated out of the equations, leading to the following two equations to be solved

$$
\begin{aligned}
&[M_{qq}]^e \{\ddot{q}\}^e + [\tilde{K}_{qq}]^e \{\Delta q\}^e = \{f_q^a\}^e - \{\tilde{f}_q^i\}^e \\
&-[D_{\vartheta\vartheta}]^e \{\dot{\vartheta}\}^e + [\tilde{K}_{\vartheta\vartheta}]^e \{\Delta\vartheta\}^e = \{f_\vartheta^a\}^e - \{\tilde{f}_\vartheta^i\}^e,
\end{aligned}
\tag{45}
$$

with

$$
\begin{aligned}
[\tilde{K}_{qq}]^e &= [K_{qq}]^e - [K_{q\alpha}]^e ([K_{\alpha\alpha}]^e)^{-1} [K_{\alpha q}]^e \\
[\tilde{f}_q^i]^e &= \{f_q^i\}^e - [K_{q\alpha}]^e ([K_{\alpha\alpha}]^e)^{-1} \{f_\alpha^i\}^e,
\end{aligned}
\tag{46}
$$

and

$$
\begin{aligned}
[\tilde{K}_{\vartheta\vartheta}]^e &= [K_{\vartheta\vartheta}]^e - [K_{\vartheta\alpha}]^e ([K_{\alpha_e\alpha_e}]^e)^{-1} [K_{\alpha\vartheta}]^e \\
[\tilde{f}_\vartheta^i]^e &= \{f_\vartheta^i\}^e - [K_{\vartheta\alpha}]^e ([K_{\alpha_e\alpha_e}]^e)^{-1} \{f_{\alpha_e}^i\}^e.
\end{aligned}
\tag{47}
$$

The element matrices and vectors in Eq. (45) are assembled into the global ones, which are denoted equally but without the superscript *e*, and the two global vectors containing the changes in displacements, rotations, electric potentials and temperature differences. The changes of the enhancing parameters are determined on elemental levels as

$$\{\Delta\alpha\} = -[K_{\alpha\alpha}]^e(\{f_\alpha^i\}^e + [K_{\alpha q}]^e\{\Delta q\}^e)$$
$$\{\Delta\alpha_e\} = -[K_{\alpha_e\alpha_e}]^e(\{f_{\alpha_e}^i\}^e + [K_{\alpha\vartheta}]^e\{\Delta\vartheta\}^e) \quad (48)$$

5. NUMERICAL EXAMPLES

We start from a thermo-piezo-elastic problem proposed in [13], a composite layered plate consisting of a steel layer with two bonded piezoelectric layers subjected to a thermo shock by rapidly cooling down the top surface (see Fig.2).

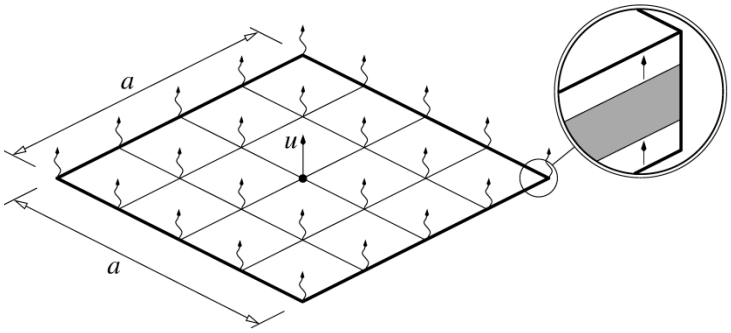

Fig. 2 Steel plate with two piezoelectric layers

A circumferentially hinged 2 cm thick 200 cm× 200 cm steel plate is covered on the top and the bottom with 0.5 cm thick piezoelectric layers as shown in Figure 2. The material properties of steel are assumed to be $E = 2.1\cdot10^{11}$ N/m^2, $v = 0.3$, $\alpha_T = 1.2\ 10^{-5}$ 1/K, $\lambda = 60$ W/mK, $c_E = 420$ J/kgK and $\rho = 7850$ kg/m^3. The material properties of the piezoelectric material are $E = 2.0\ 10^9$ N/m^2, $v = 0.25$, $\alpha_T = 6.67\ 10^{-6}$ 1/K, $\lambda = 1$ W/mK, $c_E = 420$ J/kgK, $\rho = 7600$ kg/m^3, $e_{13} = -0.5333$ C/m^2, $e_{51} = 0.1333$ C/m^2, $\delta = 1.0\cdot10^{-7}$ C^2/Nm^2, and $f = 0.25\ 10^{-3}$ C/m^{2}K (pyroelectric coefficient). The polarisation direction of the piezoelectric layers is indicated in Fig. 2 by arrows. The bottom surfaces of the piezoelectric layers are grounded.

In [13] the response of this plate has been investigated, when the temperature of the top surface is rapidly cooled down according to $T = (293.15 - 70\ (1 - e^{t/s}))$K. Here, we subject the top surface to an impulsive temperature shock according to $T = -70\cdot t\cdot e^{(1-t)}$ K. This prescribed temperature function can be seen as the line for the temperature difference at the upper surface (indicated by a "+" sign) in Fig. 4. The lower surface is assumed to be adiabatic.

Due to the temperature difference in the upper and the lower regions of the plate, bending moments are generated, which force the plate to bend downwards as shown in Figure 3. The transverse displacement at the centre of the plate is displayed according to geometrically linear and nonlinear analysis. It can be seen that the geometrically linear plate theory overpredicts the plate deformations by far. The linear

theory does not account for the stress stiffening effect, i.e. for the development of tensile forces in the plate when the deflections become large.

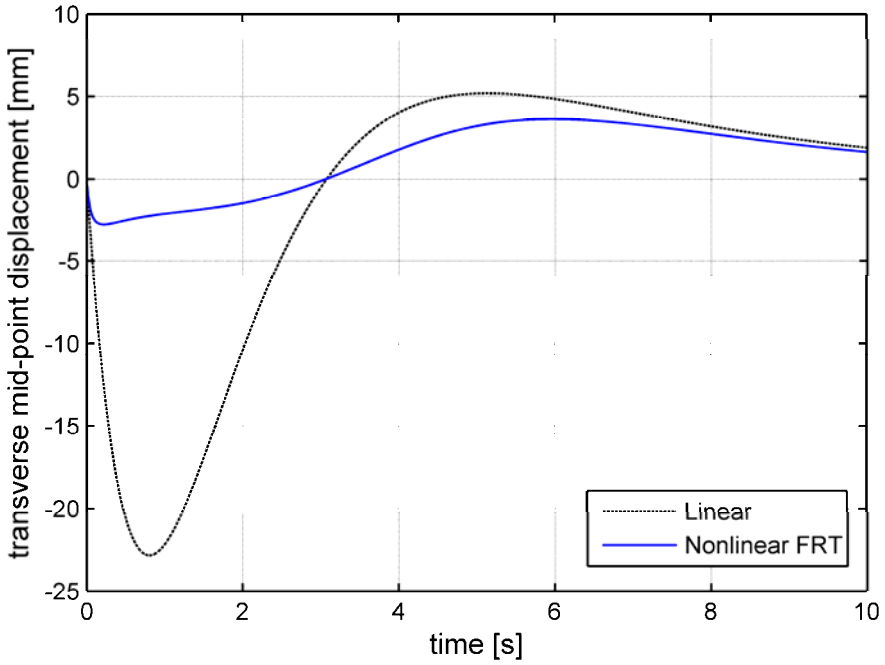

Fig. 3 Transverse displacement of the thermally loaded plate at its mid-point.

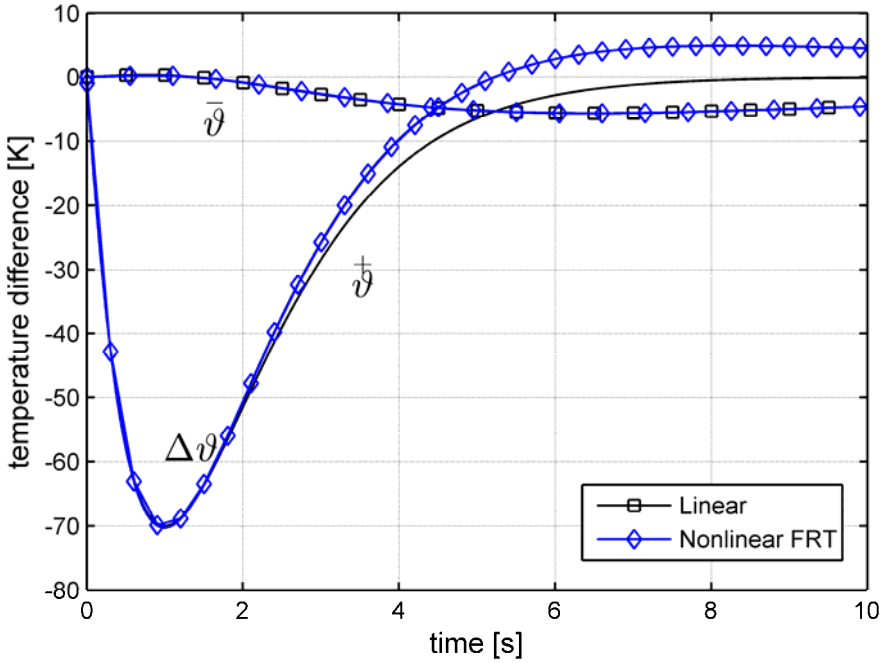

Fig. 4 Temperatures at the top and bottom surface in the plate center

It is interesting to note that the plate first bends downward, but later in the opposite direction. An explanation for this response can be found in Figure 4, which shows the

temperatures at the top and bottom surfaces of the plate and the difference $\Delta\vartheta$ between the temperature on top and bottom.

It can be seen that after the impulsive temperature shock on the top surface, due to the transverse heat conduction, the temperature on the bottom surface follows the one on the top surface with a delay inversely proportional to the heat conduction coefficients. When the prescribed temperature at the top surface rises, it happens that at a certain moment it becomes higher than that on the cooled lower surface. Thus the temperature difference $\Delta\vartheta$ changes its sign and reverse bending starts.

For a more detailed interpretation Figure 5 shows the temperature distribution through the thickness at equidistant times in increments of 1 s varying from 1 s to 10 s. After 1s the temperature on the top surface has decreased by -70 K and is than increased subsequently. It can be seen that the temperature profile at 4 s shows already lower temperatures in large parts of the lower region of the plate than in the upper one, which explains the reverse bending.

It can be noticed also in Figure 3 that for larger times the bending tends to zero. From Figure 5 it can be seen that this happens when the temperature profile shows almost equal temperatures through the thickness. Due to this compensation, the bending moments diminish in the course of time. The adiabatic boundary conditions can be noticed from the vanishing transverse temperature gradient on the bottom of the plate.

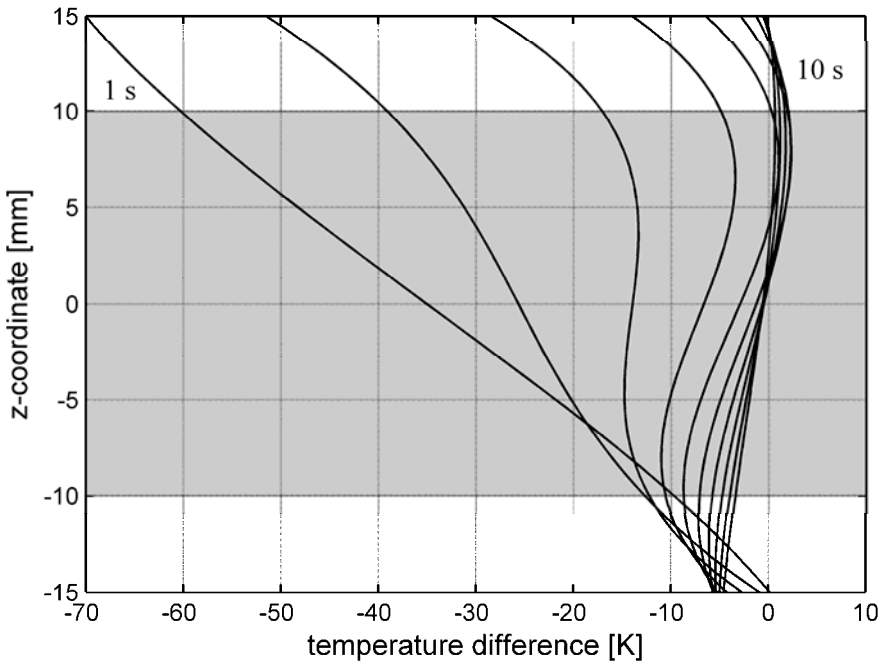

Fig. 5 Temperature distribution through the thickness at the plate center

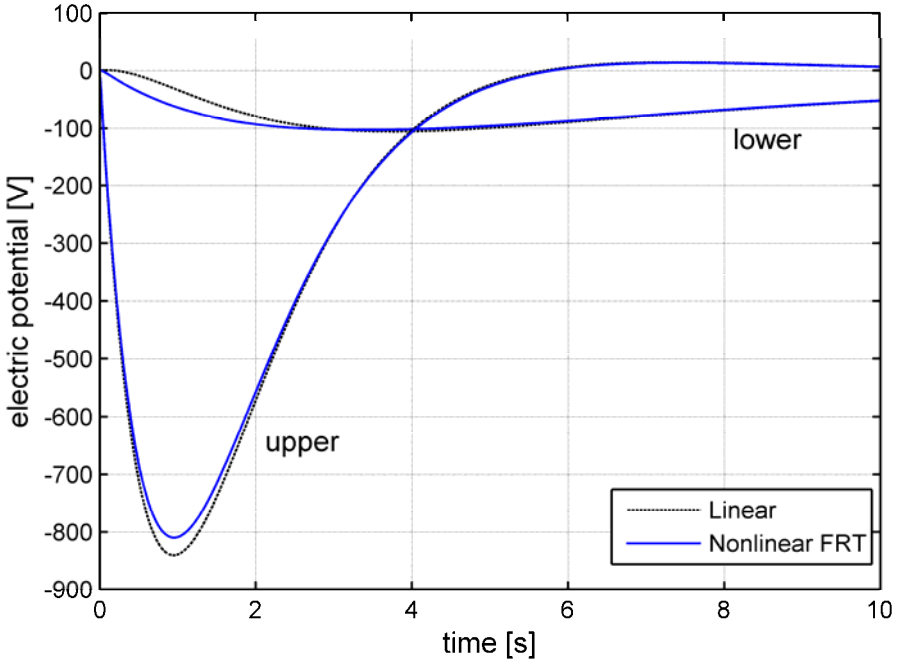

Fig. 6 Electric potentials of the upper and lower piezoelectric layers

Figure 6 shows the electric potentials on the top surfaces of the upper and the lower piezoelectric layers at the centre of the plate. When comparing the results in Figure 6 with those in Figure 4, it can be concluded that the electric potential behaves roughly proportionally to the temperature difference. For larger times the temperature difference on the top surface remains more or less constant, but due to the decreasing temperature difference between the top and bottom regions of the plate the deformations decrease to the initial state. Thus the potentials in both piezoelectric layers tend to zero.

CONCLUSION

Based on a thermodynamically consistent approach a nonlinear thermo-piezo-elasticity theory has been developed in which all coupling effects between the thermal, electrical and mechanical quantities have been taken into account. The second principle of thermodynamics has been used to derive the restrictions for the constitutive equations. Using nonlinear finite element analysis the various coupling effects have been demonstrated for a thin-walled plate with piezoelectric layers bonded to the upper and lower surface.

REFERENCES

[1] R. Schmidt, ”A Thermodynamically Consistent Theory of Elastic Plates and Shells at Finite Displacements and Rotations of the Surface Director”, Habilitation Thesis, University of Wuppertal, Germany, 1993.

[2] H. Bossong, S. Lentzen, R. Schmidt, ”Nonlinear thermoelastic analysis of thinwalled structures”, in: Computational Methods for Coupled Problems in Science

and Engineering II, eds. E. Onate, M. Papadrakakis, B. Schrefler, 457- 460, International Center for Numerical Methods in Engineering (CIMNE), Barcelona 2007.

[3] H. Bossong, S. Lentzen, R. Schmidt, ”Coupled thermo-elastic nonlinear finite element analysis of thin-walled structures”, Proceedings of the Eleventh International Conference on Civil, Structural and Environmental Engineering Computing, St. Julians, Malta, 18 - 21 September 2007, ed. B.H.V. Topping, Paper 100, Civil-Comp Press, Stirling, Scotland, 2007.

[4] H.F. Tiersten, ”On the nonlinear equations of thermoelectroelasticity”, Int. J. Eng. Sci., 9,587-604, 1971.

[5] W.K. Nowacki, ”Some general theorems of thermopiezoelectricity”, Journal of Thermal Stresses, 1, 171-182, 1978.

[6] A. Görnandt, U. Gabbert, ”Finite element analysis of thermopiezoelectric smart structures”, Acta Mechanica, 154, 129-140, 2002.

[7] S.N. Ahmad, C.S. Upadhyay, C. Venkatesan, ”Linear and nonlinear analysis of a smart beam using general electrothermoelastic formulation”, AIAA Journal, 42, 840-849, 2004.

[8] S.N. Ahmad, C.S. Upadhyay, C. Venkatesan, ”Electro-thermo-elastic formulation for the analysis of smart structures”, Smart Mater. Struct., 15, 401-416, 2006.

[9] S. Lentzen, R. Schmidt, ”A fully-coupled nonlinear thermoelectromechanical model for piezolaminated smart structures”, Proceedings in Applied Mathematics and Mechanics, 7, 4070027 -28, 2007.

[10] S. Lentzen, R. Schmidt, ”Geometrically, electrically and thermally nonlinear thermopiezomechanics”, Proceedings of the First Seminar on the Mechanics of Multifunctional Materials, Essen 2007, eds. J. Schröder, D. Lupascu, D. Balzani, 83 - 86, University Duisburg-Essen, Institute of Mechanics, 2007.

[11] S. Lentzen, R. Schmidt, ”A thermoelectromechanical model for the analysis of smart structures”, in: ”ComputationalMechanics”, Proceedings of the 8 th World Congress of Computational Mechanics / 5 th European Congress on Computational Methods in Applied Sciences and Engineering, Venice, Italy, 30 June - 4 July 2008, eds. B.A. Schrefler, U. Perego, International Center for Numerical Methods in Engineering (CIMNE), Barcelona 2008.

[12] S. Lentzen, R. Schmidt, ”Nonlinear coupled FE-simulation of thermoelectromechanical processes in thin-walled structures”, Proceedings XXII International Congress of Theoretical and Applied Mechanics, Adelaide, Australia, 25 – 29 August 2008, eds. J. Denier, M.D. Finn, T. Mattner, Adelaide 2008.

[13] S. Lentzen, ”Nonlinearly Coupled Thermopiezoelectric Modelling and FESimulation of Smart Structures”, PhD Thesis, RWTH Aachen University 2008, Fortschritt-Berichte VDI, Reihe 20, Nr: 419, VDI Verlag, Dsseldorf 2009.

[14] F. Gruttmann, W. Wagner, ”Structural Analysis of composite laminates using a mixed hybrid shell element”, Comput. Mech., 37, 2006, 479-497.

[15] L.M. Habip, "Theory of Elastic Shells in the Reference State", Ingenieur-Archiv 34 (1965), 228-237.

[16] I. Kreja, R. Schmidt, "Large Rotations in First-Order Shear Deformation FE Analysis of Laminated Shells", International Journal of Non-Linear Mechanics 41 (2006), 101-123.